

Liquid crystal based active optics

Brett E. Bagwell^{*a}, David V. Wick^a, Robert Batchko^b, Justin D. Mansell^c, Ty Martinez^d,
Sergio R. Restaino^d, Don M. Payne^e, Jamie Harriman^f, Steve Serati^f, Gary Sharp^g,
Jim Schwiegerling^h

^aSandia National Laboratories, PO Box 5800, MS 1188, Albuquerque, NM 87185-1188;

^bHolochip, 1009 Bradburry SE, Suite 05, Albuquerque, NM 87106

^cMZA Associates Corporation, 2021 Girard SE Ste. 150, Albuquerque, NM 87106-3140

^dNaval Research Laboratory, c/o AFRL/DES, 3550 Aberdeen Ave SE, Kirtland AFB, NM 87117

^eNarrascape, 737 Loma Vista Dr. NE, Albuquerque, NM 87106

^fBoulder Nonlinear Systems, Inc., 450 Courtney Way, Lafayette, CO 80026

^gColorlink, 5335 Sterling Drive, Suite B, Boulder, CO 80301

^hUniversity of Arizona, College of Optical Sciences, 1630 E. University Blvd., Tucson, AZ 85721

ABSTRACT

Liquid crystal spatial light modulators, lenses, and bandpass filters are becoming increasingly capable as material and electronics development continues to improve device performance and reduce fabrication costs. These devices are being utilized in a number of imaging applications in order to improve the performance and flexibility of the system while simultaneously reducing the size and weight compared to a conventional lens. We will present recent progress at Sandia National Laboratories in developing foveated imaging, active optical (aka nonmechanical) zoom, and enhanced multi-spectral imaging systems using liquid crystal devices.

Keywords: Active Optics, Liquid Crystal, Spatial Light Modulators, Zoom lenses

1. INTRODUCTION

Liquid crystal (LC) devices are quickly finding their way into systems as active phase modulators and optical bandpass filters in order to improve imaging capability and flexibility. Our group has been at the forefront of active imaging system, using active optics to increase field of view, vary magnification, and spectrally resolve images without moving components. The active optical components described in this paper rely on birefringent liquid crystal materials to alter either the phase or the polarization of the incoming wavefront. LC materials, as the name implies, occupy a phase state in between an isotropic liquid and an anisotropic crystalline solid. The sub-class of LC material for the devices described here are Nematic (NLC), which are uniaxial birefringent. The application of an external E field induces a dipole in the NLC molecule, which in turn interacts with the external electric field to produce a torque and a rotation of the optical axis. An incident wavefront will experience an optical path difference (OPD) that is dependent on the orientation of the NLC molecule, or, in the case of active bandpass filters, the polarization of the wavefront is rotated. To prevent migration within the LC material, NLC's are driven by an AC voltage. Since the dipole moment is induced, not permanent, it changes sign with a change in sign of the external electric field, and the torque retains its direction. The LC molecule stops its rotation when the torque exerted by the external electric field is balanced by the elastic torque exerted by the surrounding LC molecules [1].

2. LC LENSES

Liquid crystal lenses are made with either patterned electrodes or gradient polymers in order to produce an inhomogeneous electric field across the LC material [2,3]. The goal is to produce a tunable lens with electrically controllable focal length. The liquid crystal lenses discussed here employ an Aluminum circular electrode surrounded by two transparent indium tin oxide (ITO) electrodes. In between these conducting layers are glass insulators and the

* bbagwel@sandia.gov, ph. 505 284-5639

liquid crystal layer itself, as shown in Figure 1 below. The LC molecules are all aligned with their extraordinary indices of refraction oriented parallel to the x-axis. Two AC square waves are applied to the device, one between the top and bottom ITO electrodes (V_1), and one between the circular electrode and the bottom ITO electrode (V_2).

The square waves are 100 Hz in frequency and are in phase. The resultant electric field varies radially. An incident plane wave experiences maximum retardance at the lens center, and less at the edges. Ideally we want to achieve a quadratically varying phase profile given by $\phi = \exp[-ik(x^2+y^2)/2f]$. Besides voltages V_1 and V_2 , there are several additional factors that determine how closely each LC lens approximates this desired phase profile, including: LC layer thickness, glass thickness, aperture diameter, and desired focal length.

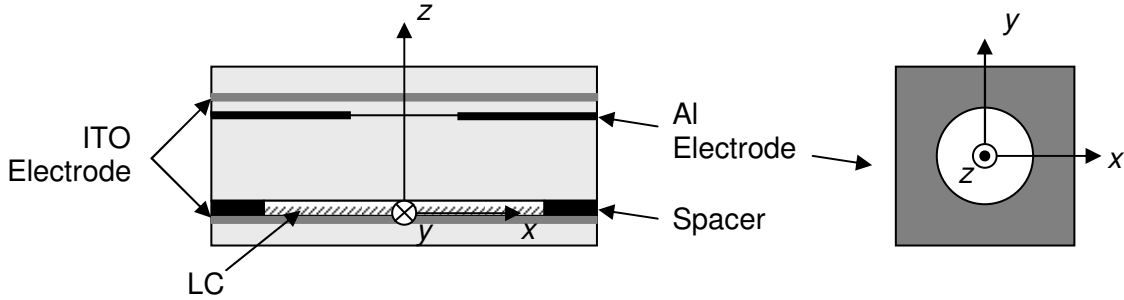
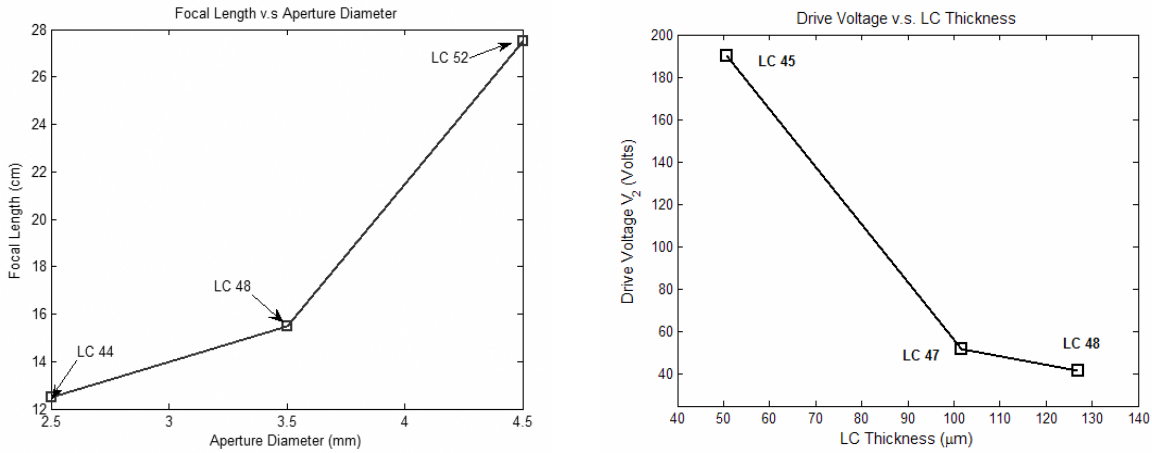


Figure 1. Liquid crystal lens.

The relationship between the diameter of the hole patterned electrode and drive voltage to achieve a specific focal length is graphically illustrated in Figure 2 (a). As the aperture increases with fixed voltages/thicknesses, the focal length also increases as expected. When one increases the LC layer thickness, keeping the other physical parameters constant, a larger drive voltage is required to maintain a fixed focal length, as shown in Figure 2(b).



(a). $V_1 = 20$, $V_2 = 50$, Thickness = 127 μm . (b). $V_1 = 20$, $f = 20$ cm, Dia. = 3.5 mm.

Figure 2. Relationship between aperture diameter, effective focal length, V_2 , and LC thickness

HoloChip, LLC provided us with 12 lenses, 3 different diameters ranging from 2.5mm to 4.5mm and 4 thicknesses ranging from 51 μm to 127 μm . We evaluated six of those lenses by varying the drive voltages (V_1 : 20-100V and V_2 : 50-250V). We measured the wavefront error and relative on-axis irradiance and decided to fix V_1 at 20 V. We then characterized six lenses.

On-Axis Irradiance: We measured on axis irradiance relative to total incident irradiance for a given focal length. Metric: Highest relative on-axis irradiance (*light in a bucket*).

Focal Length: We varied V_2 , measuring distance at which on axis irradiance was a maximum. Metric: Minimum focal length, defined as the distance at which on-axis irradiance was at least 20% of incident.

Aberrations: We then selected two lenses with best F/# and relative on axis irradiance and obtained wavefront error for the shortest focal length. Metric: OPD < 1λ .

We illuminated the LC lens with a collimated HeNe ($\lambda = .632 \mu\text{m}$) and measured the total irradiance exiting the clear aperture. Having fixed V_1 , we then varied V_2 and measured the resulting focal length by translating a $150 \mu\text{m}$ pinhole in x, y, and z until we achieved a maximum reading on the detector/power meter. As we reduced the focal length, aberration increasingly blurred the focused spot. We defined the minimum focal length as the distance at which this maximum was at least 20% of the total irradiance measured in an unpowered state.

Figure 3 depicts the result for five of the most promising LC lenses. Based on their relatively short focal lengths and high on-axis irradiance, we selected LC lenses 47 and 48 for further characterization.

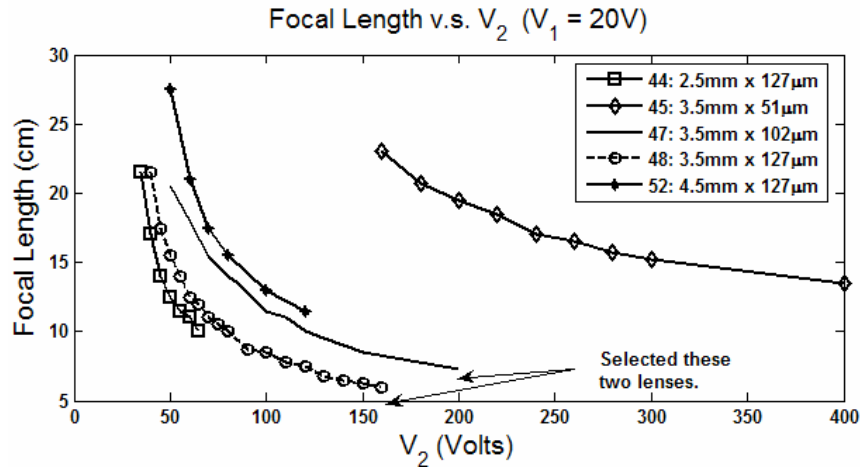


Figure 3: Focal Length versus. V_2

To quantify the wavefront error of the LC lenses, we set up the LC lenses in front of a Zygo with a positive reference sphere. By placing the focused spot from this reference sphere at the front focus of the LC lens and then reflecting the collimated light off a flat mirror we were able to create an external reference leg. In order to enable measurements at various focal lengths we inserted a positive lens on a translation stage between the flat mirror and the LC lens. When power is applied to the LC lens, the distance that this positive lens needs to be moved to re-collimate the light onto the flat mirror is given by:

$$\Delta Z = \frac{(Z_o)^2}{f_{LC} - Z_o}$$

To independently verify our previous focal length measurements, we applied the appropriate V_1 and V_2 voltages, and translated the positive lens until the OPD was a minimum. Measuring Δz , we then calculated and compared the *short* focal lengths for LC 47 and 48, with the following results. The aberrations for the minimum focal length for each lens are shown below in Figures 4 and 5.

LC 47	Irradiance	OPD	LC 48	Irradiance	OPD
	7.3 cm	7.0 cm		7.0 cm	7.15 cm
	8.5 cm	8.5 cm		7.8 cm	8.0 cm
	10.0 cm	9.96 cm		10.0 cm	9.8 cm

Table 1. Comparison of the focal lengths of two liquid crystal lenses using irradiance and OPD measurements.

3. LC SPATIAL LIGHT MODULATORS

At a molecular level the LC SLM operates on exactly the same principles as the LC lenses. They utilize birefringent liquid crystals, an AC external electric field, and an induced dipole moment from that electric field, to rotate the parallel aligned molecules in the axis of polarization. However, the OPD is adjusted by changing the index of refraction on a pixel-by-pixel basis [4], see Figure 6. Because they are pixilated, SLMs have more flexibility than LC lenses and can be used to compensate higher order wave front aberrations. However, they suffer from a reduction in signal (throughput) and an increase in noise (diffraction artifacts) due to the opaque transistors surrounding each pixel. These opaque areas are necessary because of the transistors required to locally vary the electric field, see Figure 7.

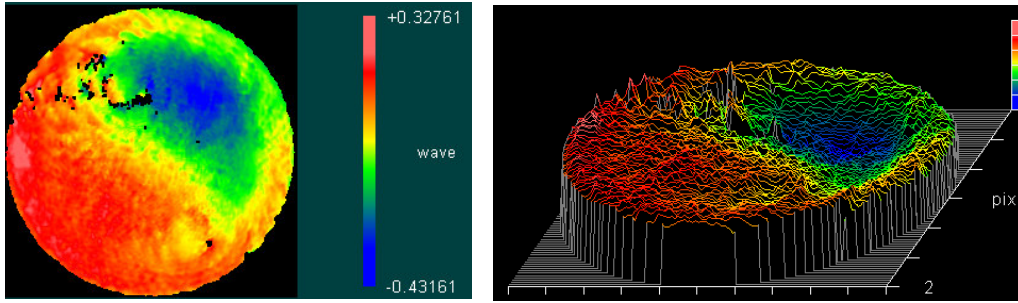


Figure 4: OPD LC 47, $f = 10$ cm. $W_{pv} = 0.75 \lambda$

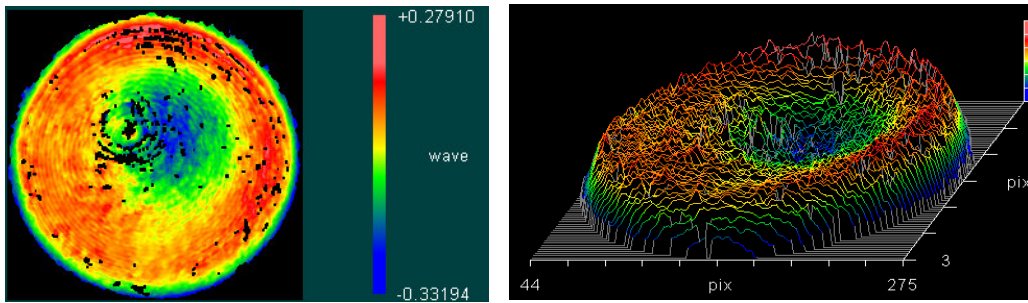


Figure 5: OPD LC 48, $f = 7$ cm. $W_{pv} = 0.61 \lambda$

The LC layer in an SLM is also typically much thinner (order(s) of magnitude) than an LC lens, which enables faster response times, but limits the maximum OPD. These devices are typically designed to achieve a 2π phase depth, and therefore wavefront compensation is accomplished modulo- 2π . For a reflective LC SLM this is reduced by half, via a double pass at each pixel, necessitating much less LC material. The most significant limitation imposed by pixilation of the phase map, is on the achievable phase gradient of the LC SLM. Spatial light modulators quantize the desired phase correction (electronic addressability) and sample it spatially (pixel size). All of the spatial light modulators that we used were fabricated by Boulder Nonlinear Systems, Inc. and had 8 bits of phase addressability (per 2π). This exceeded the spatial resolution of the LC pixels, and thus *sampling was our limiting constraint*.

Both the LC lenses and the LC SLM suffer from chromatic aberrations due to dispersion. However, the bandwidth on the LC SLMs is an further restricted by an order of magnitude due to the modulo- 2π operation. Modulo- 2π is only accurate at a single wavelength, and as we move away from that central wavelength, chromatic aberrations quickly become very pronounced. Thus, LC SLMs can only be used over narrow wavelength bands. However, since LC SLMs have fast response times, the phase correction can be changed at rates greater than 30 Hz. When used in conjunction with PIFs (see below), this gave us the ability to image various wavelength bands (e.g. RGB) at near video rates.

The LC molecular rotation is a non-linear function of pixel voltage, and the index of refraction is a non-linear function of wavelength [4]. Thus the LC SLM must be characterized at each voltage for each wavelength of interest, in this case $\lambda_N = .486, .532, \text{ and } .632 \mu\text{m}$. The end result of any effort at characterization is a voltage look-up table that takes a linear input (desired phase/8 bit integer) and applies the appropriate voltage to achieve the correct amount of rotation for a linear phase at the output:

The voltage at a pixel location, is given by the difference between the transparent top plane (always 2.5 Volts) and the reflective backplane. The voltage on the backplane pixel is determined by an (8 bit) .bmp file, and thus the top and bottom potential difference is:

$$\Delta V = \left(\frac{\text{Grayscale}}{255} \right) \cdot 5V - 2.5V$$

For example, a pixel programmed with grayscale 0 (or 0 Volts) would produce a maximum electric field (of 2.5 V) across the liquid crystal. A pixel programmed with grayscale 255 (5 Volts) would produce a difference of -2.5 V across the LC. Due to the polarity independence of the LC rotation, 8 bits over 5 V actually limits us to 7 bits (128 levels) of phase response.

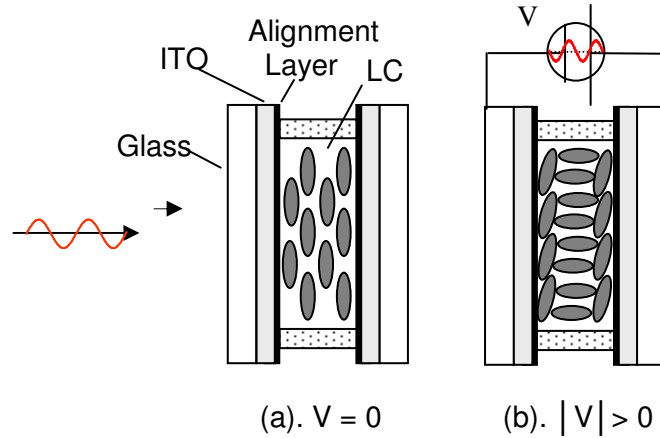


Figure 6: LC SLM Molecular Orientation

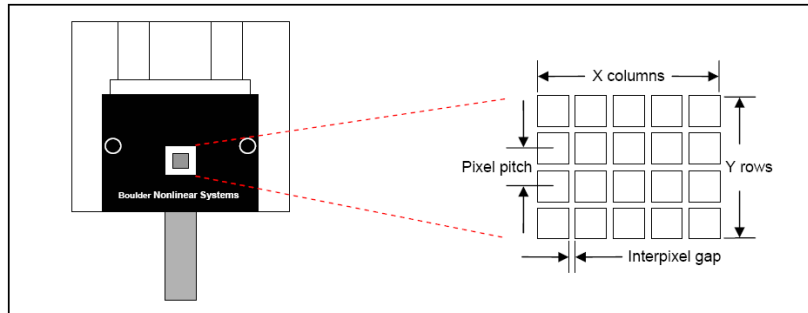


Figure 7: LC SLM Pixilation Scheme

4. POLARIZATION INTERFERENCE FILTERS

Polarization interference filters rely on birefringent materials placed between a polarizer and analyzer. This birefringence performs both the wavefront shearing and OPD necessary for interference of a linearly-polarized input, while the analyzer provides the requisite recombination. The number of birefringent layers, layer thicknesses, amount of birefringence, and orientation relative to the polarizer and analyzer dictate the pass-bands.

Filters have been constructed that are simply the addition of multiple such stages, each of geometrically increasing retarder thicknesses but with the same birefringence and orientation, a concept first described by B. Lyot in 1933 [5]. Solc et.al, later improved upon the basic Lyot design by introducing multiple retarders between a single polarizer and analyzer, albeit with different birefringent orientation [6]. With the addition of birefringent LC material in the individual stages of both types of filters, the narrow spectral pass-band of the filter can be tuned via an applied voltage [7].

Commercial devices based on both Lyot and Solc analog filters are currently available. In general, analog bandpass filters based on the Lyot and solc designs suffer from significant drawbacks for our applications of interest including throughput, filter thickness, and field-of-view. The polarizing film in each filter stage typically has approximately a 10% transmission loss. Filters with high finesse and acceptable dynamic range generally have poor peak transmission and are bulky. In the Solc filter, bandpass tunability requires that each multi-order retarder is fully tunable. So in practice, throughput is often not significantly improved, because the insertion loss of each polarizer is traded for the additional LC cell losses. A more viable alternative has been developed by ColorLink, Inc. for use in the VIS, with the potential for extension to the NIR and SWIR.

Digital Tunable Filters (DTFs)

DTFs use digitally driven LC devices as wavelength-neutral polarization switches for the random-access selection between a pre-defined set of spectral profiles. Like the Lyot filter, DTFs represent the product of independent filter stages. However, the task of generating a high-quality bandpass is almost exclusively confined to a single element: a Solc-type passive retarder stack (RS) placed in each stage. The retarder stack is typically a multi-layer laminate of bulk transparent stretched polymer (birefringent) retarder films. The LC layer simply provides (digital) access to the passband of each retarder stack.

Unlike the LC material in the SLMs and lenses, this LC layer has its front and back alignment layers with orthogonal orientations. The result is that the bulk orientation of the LC molecules n_c axis rotates helically through 90° , a configuration known as twisted-nematic (TN). The wave guiding effect this has on a LP input is that exploited for amplitude modulation in LC displays. In this case, when a 90° TNLC polarization switch is placed directly adjacent a retarder stack, between polarizing films, the spectrum can be electronically switched between a band-pass spectrum and the complementary notch spectrum. It is not unusual for a driven TN device between crossed polarizers to have a light leakage below 0.1% (at normal incidence). The localization of the filtering to the retarder stack reduces complexity/size and eliminates calibration [8].

It is generally the case that nematic LC devices operated as digitally switched elements have one voltage state that is substantially more/less chromatic than the alternate state. A 90-degree TNLC device has a self-compensation feature, such that the driven state is very nearly isotropic. Conversely, it requires substantial effort to design a TN device that provides a wavelength independent conversion of input linearly polarized light to the orthogonal polarization. Practically, TN devices with reasonable switching speed have a relatively high degree of chromaticity to their polarization conversion spectrum. This has the effect of compromising the performance of the retarder stack, most notably by reducing dynamic range. The driven state is thus used to generate the bandpass profile, such that this spectrum is minimally compromised [8].

For our applications, ColorLink's designed a visible DTF, customized with an additional passive (Solc type) PIF, that narrows the bandwidth of each channel from the active stage. The clear aperture of this device is 35 mm, the total thickness (passive and active stages) is 15 mm, and it accepts a cone angle of F/2.2 or higher (HFOV $\leq 13^\circ$). Spectral response curves for the active and passive stages are shown below in Figures 8 and 9. The combined transmission spectrum is shown in Figure 10. Note that at towards longer wavelengths (> 800 nm), the polarizers within the DTF and PIF become isotropic, and thus no interference occurs. This necessitated the addition of an NIR cut-off filter.

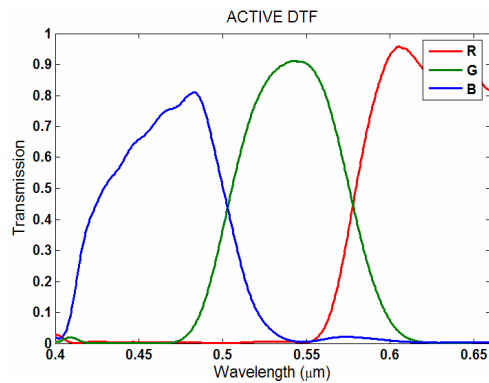


Figure 8: Digital Tunable Filter (DTF) pass-bands

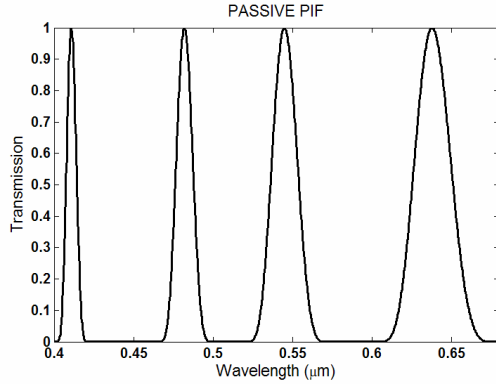


Figure 9: Passive Polarization Interference Filter (PIF) pass-bands

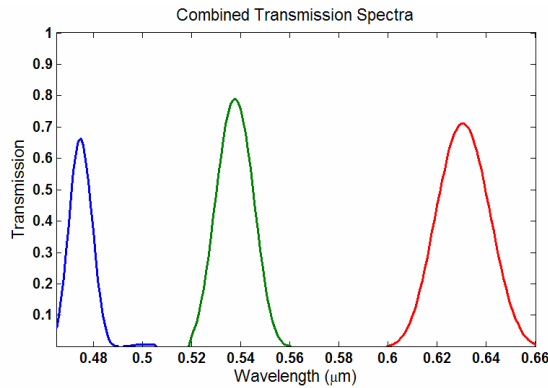


Figure 10: Combined transmission from DTF and PIF “Blue”: 475 ± 5 nm. “Green”: 538 ± 9 nm. “Red”: 631 ± 13 nm.

5. ENHANCED SPECTRAL BANDWIDTH

Axial (or longitudinal) chromatic aberration is simply a variation in focal length $f(\lambda)$ with wavelength. In addition to the spectral response of the focal plane array/film, it is often the limiting factor determining the useable spectral bandwidth of a transmissive system, especially near the optical axis [9]. In the case of a positive refractive lens, shorter wavelengths will have a shorter focal length than longer wavelengths. Wherever we place the image plane, all but one of the wavelengths will be out of focus (at least in the geometric approximation), as shown below in Figure 11.

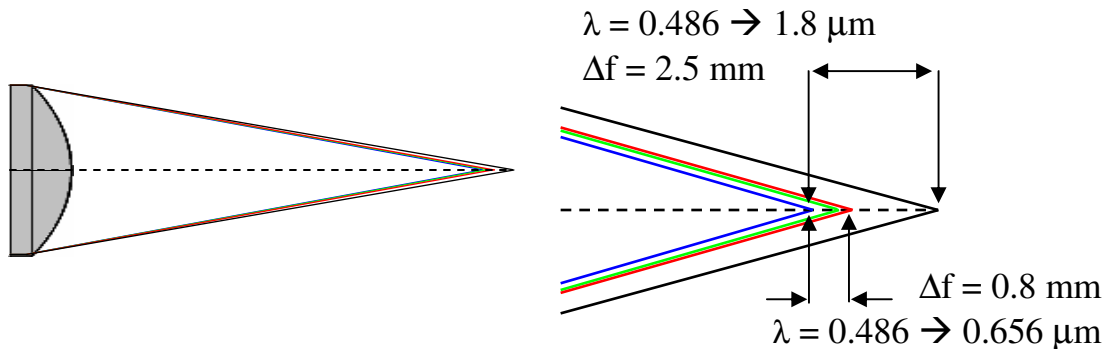


Figure 11: Axial Chromatic Aberration in an F/2, BK7 Singlet

Further image degradation associated with dispersion results from transverse chromatic aberrations and the wavelength dependence of the so-called monochromatic aberrations (especially at large field angle) [10]. Traditionally, more lenses with different glass types are added in order to increase the spectral bandwidth over which the system meets some required metric (e.g. diffraction/detector limited, minimum spatial resolution, etc.). Mechanical color wheels can also be used in tandem with an adjustable focus if spectral discrimination is desired, typically over a narrow field of view.

We have developed and demonstrated an alternate solution using liquid crystal (LC) based polarization interference filter (PIF) to isolate a narrow spectral region of interest and LC lenses to correct the aberration (defocus) over that spectral region. The end state is a transmissive system that is compact, requires no macro-moving parts, and has the ability to spectrally resolve an image. Preliminary images from this simple imaging system consisting of a single BK7 lens and utilizing the DTF from Colorlink as a dynamic spectral filter and the LC lens from Holochip to correct for longitudinal focus are shown below. Note that at 0.45μm the LC lens is off and the system is aligned for best focus.

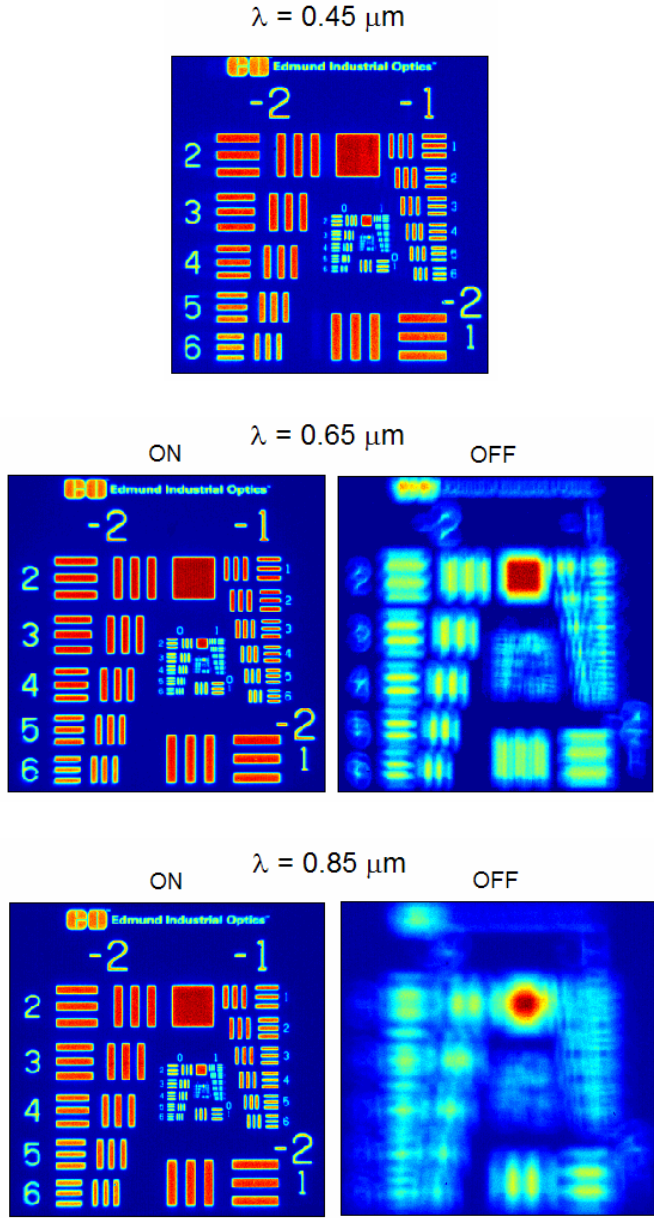


Figure 13: Resolution target images at the design wavelength (450nm), 650nm, and 850nm with and w/out correction

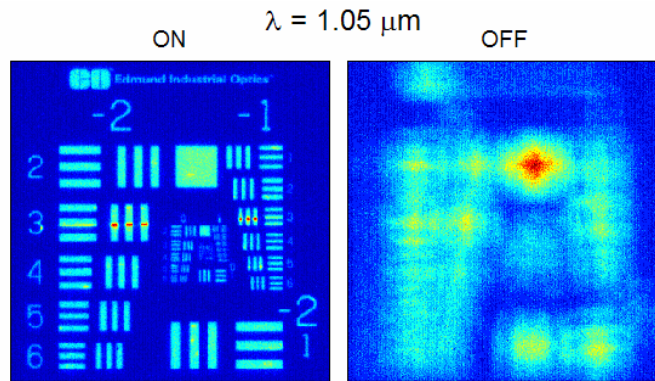


Figure 14: Resolution target images at 1.05 μm with and without spectral correction

6. FOVEATED IMAGING

When designing a wide field-of-view (FOV) lens, an optical designer is faced with the challenge of maintaining high image quality across the entire FOV while achieving specific metrics such as F/#, entrance pupil diameter, and overall length. Complex designs utilizing multiple optics are typically used in fast (i.e. low F/#) systems to minimize off-axis aberrations, but even the best, well-corrected systems have a limited FOV. Because of the multiple optical elements that are required, these systems are often heavier and bulkier than narrower FOV systems. The complexity can be minimized with a slower system but at the expense of either light gathering ability or overall length.

To minimize the complexity and maintain a low $f/\#$ (i.e. fast system), active optical elements can be used to correct the wave front in the pupil plane of a simple optical system with a wide FOV. This correction is only valid for a narrow portion of the entire FOV, the instantaneous field of view (IFOV), but its location can be changed according to the user needs. The term “foveated” imaging originates from the operation of the human eye, where a limited area within a few degrees of the point of gaze is highly resolved and resolution falls off rapidly with increasing field angle. Wave front correction to better than $\lambda/2$ for 2 and 3 element systems out to $\pm 30^\circ$ has previously demonstrated [11,12].

The limitation of this configuration is that the phase correction is done modulo- 2π . As discussed previously, this means that the applied phase map is valid at only one wavelength (or narrow range of wavelengths). In order to image multiple wavelengths, in a manner that is consistent with our program goals (smaller, lighter weight, non-mechanical, wide FOV) we utilized a the DTF from Colorlink in conjunction with a foveated wide field-of-view imaging system to obtain a multi spectral foveated imaging system.

Figure 15 and 16 depict static images taken with an appropriate phase correction for $\lambda = 631\text{nm}$ and 538nm , respectively at a 25° field point. For comparison, the same field point is shown in an aberrated state. The area of correction is nearly diffraction limited in both instances. Details of this experiment are presented in Reference 13.

7. ACTIVE OPTICAL ZOOM

Previously, nonmechanical zoom (NMZ) systems have been demonstrated using reflective SLMS or deformable mirrors only [14,15]. By their nature reflective components do not lend themselves to wide FOV or compact designs. Instead, we explored the range of transmissive nonmechanical zoom designs, with a minimum of two and a maximum of five optical elements.

The system we built to demonstrate the concept had only three states but was theoretically capable of continuous zooming action through the entire range. The un-vignetted FFOV for the three states was 1.0° , 2.5° , and 5.0° . While we were excited by achieving 5X magnification from a system that was 36cm long, perhaps the most exciting aspect was the ability to magnify off-axis. Off-axis imaging is displayed in Figure 17.

Note the slight degradation in image quality from the on-axis case to the edges of the field. This shift in the IFOV required increasing spatial frequency content on the SLM, eventually exceeding the Nyquist sampling rate and reducing the signal-to-noise. Nonetheless, the results were encouraging and, at a minimum, validate this unique capability embodied in a nonmechanical zoom system. This system will be described in detail in an upcoming article.

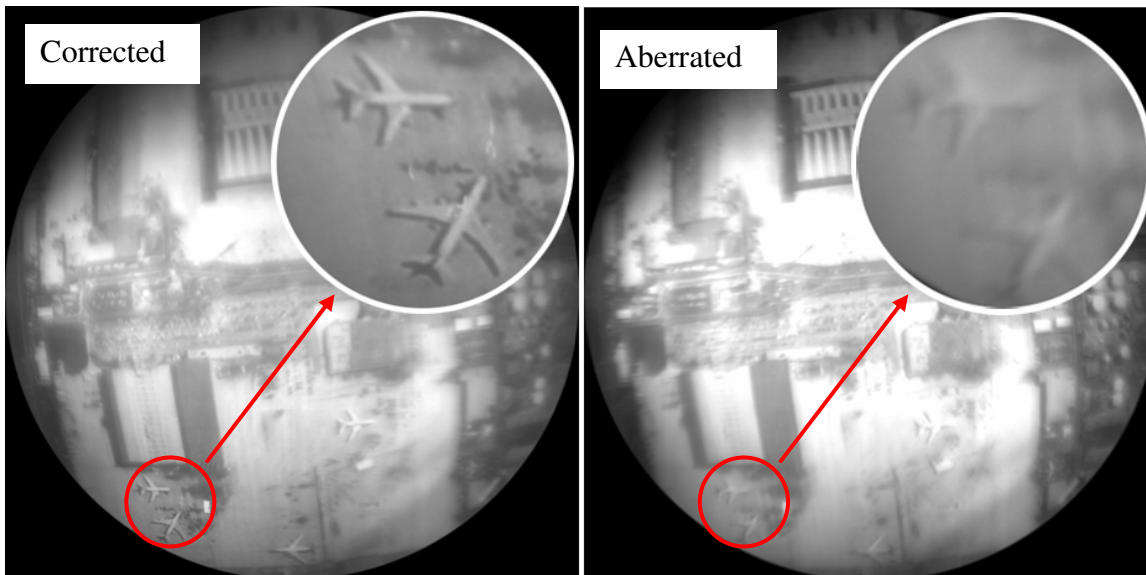


Figure 15: 25° Foveated Imaging, $\lambda_c = 631 \pm 13$ nm.

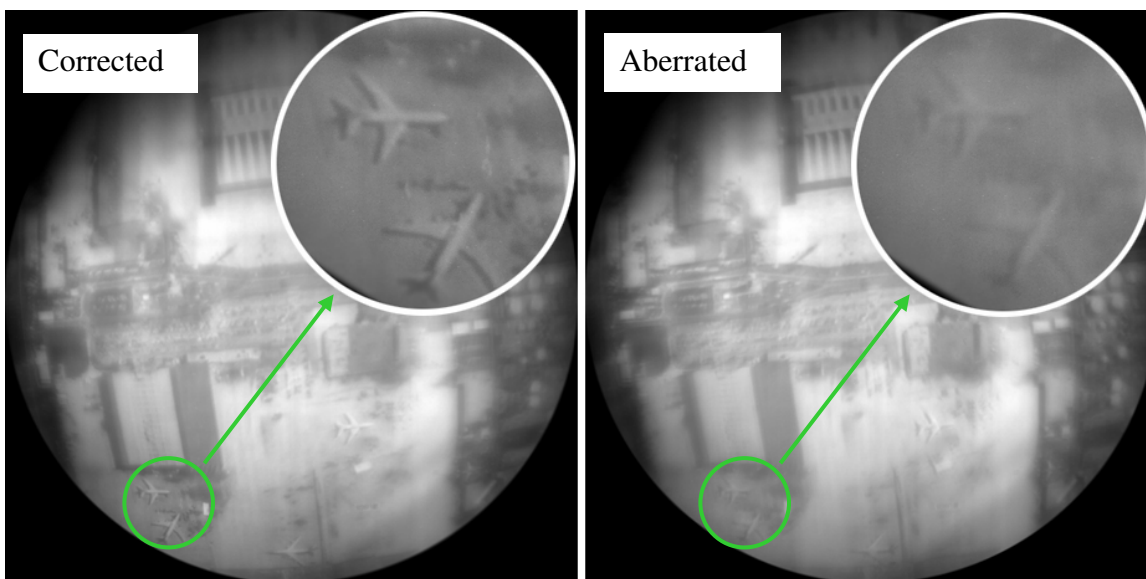


Figure 16: 25° Foveated Imaging, $\lambda_c = 538 \pm 9$ nm.

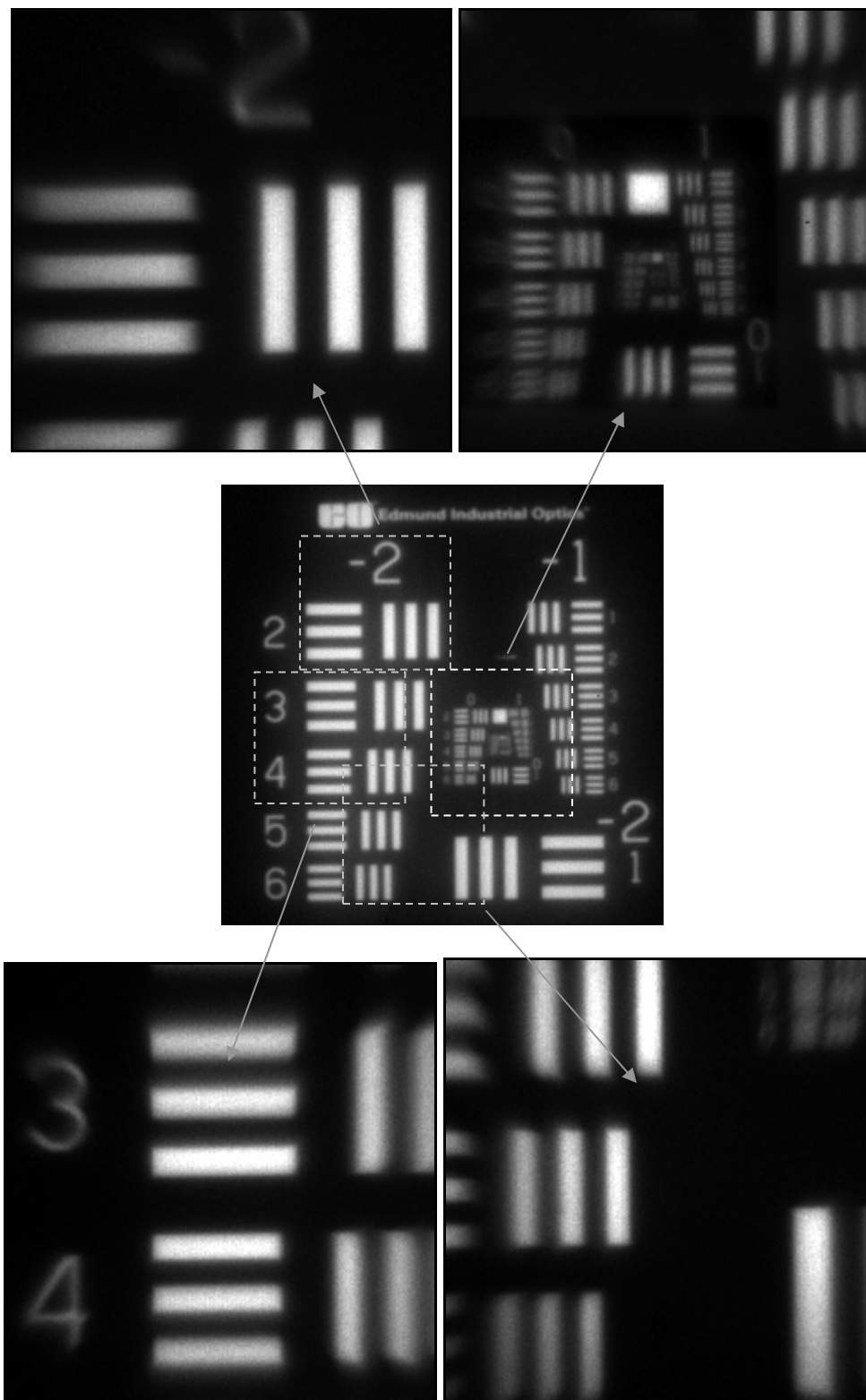


Figure 17: Off-Axis Magnification $f_{\text{EFF}} = 105 \text{ mm}$.

8. CONCLUSION

We have successfully demonstrated the use of liquid crystal spatial light modulators, lenses, and bandpass filters to: 1) increase the useable field-of-view of a simple imaging system, 2) increase the useable spectral bandwidth of a simple imaging system, and 3) increase the transverse magnification of a simple imaging system without macroscopic moving parts. Further development of active elements will result in more compact, lighter weight systems that require less power yet have greater capability than their conventional counterparts all at a lower cost.

ACKNOWLEDGMENTS

The authors would gratefully like to acknowledge the invaluable assistance of Brian Clark and useful discussions with Scott Teare, Jonathan Andrews, and Chris Wilcox. Sandia is a multiprogram laboratory operated by Sandia Corporation, a Lockheed Martin Company, for the United States Department of Energy under Contract DE-AC04-94AL85000.

REFERENCES

1. J.W. Goodman, *Introduction to Fourier Optics*. 3rd ed., Roberts & Company, Englewood, 2005.
2. A.F. Naumov, et al., "Control optimization of spherical modal liquid crystal lenses," *Optics Express*, **4**(9), 344-352 (1999).
3. M. Ye, B. Wang, and S. Sato, "Liquid-crystal lens with a focal length that is variable in a wide range," *Appl. Opt.*, **43**, 6407-6412 (2004).
4. S.T. Wu, *Nematic Liquid Crystals*. Spatial Light Modulator Technology - Materials, Devices, and Applications, ed. U. Efron. Vol. 1, Marcel Dekker, Inc., New York, 1995.
5. B. Lyot, "Optical Apparatus With Wide-Field Using Interference of Polarized Light," *C.R. Acad. Sci.*, **197**, 1593 (1933).
6. I. Solc, "Birefringent Chain Filters," *Journal of the Optical Society of America*, **55**, 621 (1965).
7. G. Kopp, M. Derks, and A. Graham, "Liquid Crystal Tuneable Birefringent Filters," *Proc. of SPIE*, **2830**, 345-350 (1996).
8. G. Sharp, (private communication).
9. W.J. Smith, *Modern Optical Engineering*. 3rd ed., Ch. 7. McGraw-Hill, New York, 2000.
10. M.J. Kidger, *Fundamental Optical Design*, SPIE, Bellingham 2002.
11. D. V. Wick, T. Martinez, S.R. Restaino, and B.R. Stone, "Foveated imaging demonstration," *Optics Express*, **10**(1), 60-65 (2002).
12. D. V. Wick, et al., "Wide-field-of-view foveated imaging system using a liquid crystal spatial light modulator," *Proc. of SPIE*, **4715**, 58-62 (2002).
13. B.E. Bagwell, D.V. Wick, and J. Schwiegerling "Multi-Spectral Foveated Imaging System," *Proc. IEEE Aerospace Conference* (2006).
14. D. V. Wick and T. Martinez, "Adaptive Optical Zoom," *Optical Engineering*, **43**(1), 8-9 (2004).
15. D.V. Wick, et al., "Active optical zoom system," *Proc. of SPIE*, **5798**, 151-157(2005).